



## High-order harmonics and supercontinua formed by a weak optical pump in the presence of an extreme terahertz field

I. Babushkin <sup>1,2,3,\*</sup> A. Demircan,<sup>1,3</sup> U. Morgner,<sup>1,3</sup> and A. Savel'ev <sup>4,5</sup>

<sup>1</sup>*Institute for Quantum Optics, Leibniz Universität Hannover, Welfengarten 1, 30167 Hannover, Germany*

<sup>2</sup>*Max Born Institute, Max Born Strasse 2a, 12489 Berlin, Germany*

<sup>3</sup>*Cluster of Excellence PhoenixD (Photonics, Optics, and Engineering - Innovation Across Disciplines), Welfengarten 1, 30167 Hannover, Germany*

<sup>4</sup>*Faculty of Physics, Lomonosov Moscow State University, Leninskie gory 2, 119991 Moscow, Russia*

<sup>5</sup>*Lebedev Physical Institute, Russian Academy of Sciences, Leninskii prospekt 53, 119991 Moscow, Russia*



(Received 3 June 2022; accepted 21 June 2022; published 28 July 2022)

We show that in the presence of an extreme terahertz (THz) field an additional weak field in the optical frequency range can modulate ionization probability and thereby generate high-order harmonics. The extreme THz pump suppresses recollisions, thereby also fully suppressing the recollision-based harmonics. Nevertheless, high-order harmonics are effectively generated via an alternative mechanism, the so-called Brunel mechanism, based on ionization and subsequent acceleration in the driving field (but not on reabsorption). Using *ab initio* simulations for the hydrogen atom and short few-cycle optical driver, we show the appearance of a coherent carrier-envelope-phase-insensitive supercontinuum formed by such harmonics, compressible into an isolated pulse with 100-attosecond-scale duration.

DOI: [10.1103/PhysRevA.106.013115](https://doi.org/10.1103/PhysRevA.106.013115)

### I. INTRODUCTION

Studies of the extreme-field terahertz (THz) interaction with matter are in their infancy due to quite a few available sources of extreme THz fields. The situation is changing currently, in particular, due to the novel sources of THz fields exceeding 100 MV/cm in 1- [1] and 30-THz [2] ranges. This allows us to consider processes appearing in the extreme-field regime at THz frequencies, such as THz-induced nonlinearity [3], generation of high-order harmonics of the THz field [4], semiconductor materials bleaching [5], and even thin-film breakdown under the action of the extreme THz pulses [6].

It is well known that for high enough optical intensities, when the atoms and molecules undergo tunnel ionization, high-order harmonic generation (HHG) appears due to the subsequent return of electrons to their parent cores [7], allowing to break the femtosecond limit for the pulse duration possessed by other techniques [8,9]. Some work was done before in the THz domain by exploring the influence of a “strong” dc or quasi-dc (THz) field on HHG by an optical field [10], on the generation of even-order high-order harmonics for imaging operating electronic circuits in the nonperturbative mode [11], and the generation of attosecond pulses [12]. Here the dc or THz field, which is not high enough to cause ionization, controls quantum paths of an electron ionized by the optical [or midinfrared (mid-IR)] pulse. In particular it was shown [13] that HHG from the intense mid-IR field (670 MV/cm) can be con-

trolled efficiently with a strong THz field (100 MV/cm at 33 THz).

The limit where the THz field can ionize atoms, molecules, and/or solids directly is of special interest since achievable THz field strengths exceed greatly the dc breaking threshold of a medium [14,15]. In particular, impact-ionization-induced transient optical nonlinearity was considered recently in *p*-Si at a THz field above 10 MV/cm [16].

It is known that the appearance of an electron in the continuum and subsequent acceleration in a strong field also lead to harmonics [17] via bound-free and free-free transitions [18,19], that is, without the need for the electron to come back. Here we will call the corresponding nonlinearity the “Brunel nonlinearity” [20,21], and the arising harmonics will be denoted “Brunel harmonics.” Note that the ionization-induced nonlinearities are “nonperturbative”; that is, one cannot obtain the harmonics as a series expansion in the vicinity of zero driver field—in contrast to a typical case of nonresonant bound-bound nonlinearities.

In this paper, we consider HHG created by a weak probe pulse at optical (in particular, mid-IR) frequencies in the presence of an extreme THz transient that is strong enough to cause a certain level of tunneling via ionization. Under these circumstances, even a weak optical probe modulates the ionization probability with optical frequency, leading to a strong nonlinear response. We observe that the strong THz driver suppresses recollision-based harmonics, making dominant the harmonics generated by the Brunel mechanism. In the situation when the optical probe has a few-cycle duration, such harmonics may form a broad coherent supercontinuum with a flat spectral phase profile, independent of the carrier-envelope phase of the optical probe, which is

\*babushkin@iqo.uni-hannover.de

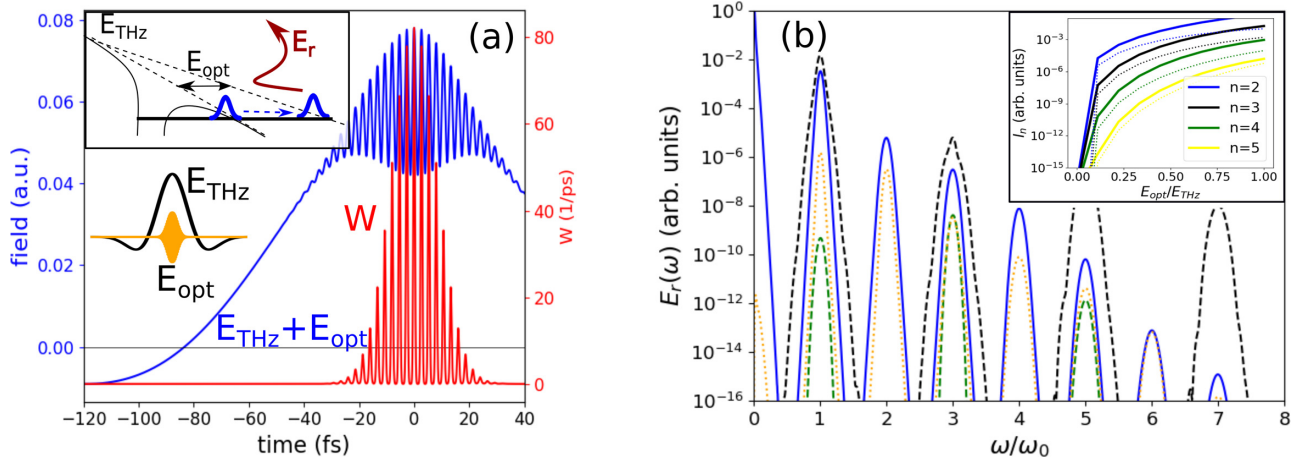


FIG. 1. Nonlinear response of argon to a weak optical probe pulse in the presence of a strong THz field—a simple-man picture. (a) Exemplary electric field (upper blue line) consisting of a strong THz field ( $E_{\text{THz}} = 0.06$  a.u.) centered at 100- $\mu\text{m}$  wavelength and a weaker fundamental harmonic at 800-nm wavelength ( $E_{\text{opt}} = 0.018$  a.u.), together with the ionization rate  $W(t)$  (lower red curve) induced by such a wave shape in argon according to the simple-man tunnel model. The lower inset shows the composition of the full driver signal from strong THz  $E_{\text{THz}}$  and weak optical  $E_{\text{opt}}$  field. The upper inset shows the schematics of the basic mechanism. (b) Corresponding Brunei harmonic response as given by Eq. (1) (blue solid line) and Brunei harmonics created by the optical field alone with the amplitude  $E_{\text{opt}} = 0.078$  a.u. [corresponding to  $E_{\text{opt}} + E_{\text{THz}}$  from (a); black dashed line] and  $E_{\text{opt}} = 0.018$  a.u. [corresponding to  $E_{\text{opt}}$  from (a); green dashed line]. The orange dotted line shows the impact from bound-bound transitions for the two-color case. The inset shows the intensity of  $n$ th harmonics (for several values of  $n$ ) depending on  $E_{\text{opt}}$  (solid lines) as well as the impact of bound-bound transitions (dotted lines).

also capable of compression to an isolated attosecond-scale pulse.

## II. SIMPLE-MAN PICTURE

To start with, we formulate our idea using a simple-man quasistatic tunnel-based model of the ionization in strong optical fields [22]. In this framework, the electron tunnels from the ground state to the continuum through the barrier created on the one side by the core potential and on the other side by the strong external driving field [see Fig. 1(a)]. Effectively, the electron can be considered as being born in the continuum with the ionization rate  $W(t) = (\alpha/|\mathbf{E}|) \exp(-\beta/|\mathbf{E}|)$ , where  $\alpha$  and  $\beta$  are some coefficients, depending on the ionization potential, and  $\mathbf{E}$  is the driving field strength [22]. The free electrons form a current [21,23,24] given, under the assumption that the initial velocity is negligible, by

$$\frac{d\mathbf{J}}{dt} = \frac{e^2}{m} \rho(t) \mathbf{E}(t). \quad (1)$$

Here  $e$  and  $m$  are the electron charge and mass, respectively, and  $W(t)$  and the free-electron density  $\rho(t)$  are connected by  $\frac{d\rho(t)}{dt} = W(t)[\rho_0(t) - \rho(t)]$ , where  $\rho_0(t)$  is the density of neutrals before the field is switched on.

The change in the current, according to the Maxwell equations, serves as a source of electromagnetic radiation  $\mathbf{E}_r \propto d\mathbf{J}/dt$ , which is here referred to as Brunei harmonics. When the initial driving pulse is a strong THz wave with intensity near the onset of the tunnel ionization, the presence of even a weak pulse at the optical frequency leads to a significant modulation of the tunneling probability at the subcycle scale and thus to a strong nonlinear response [see inset in Fig. 1(a)]. An exemplary simulation is shown in Fig. 1, where Fig. 1(a) shows the dynamics of the ionization of an argon atom ( $V_i =$

15.6 eV) for the case of the pump given by a linearly polarized THz field with a duration of 100 fs, a central frequency of 3 THz, and amplitude  $E_{\text{THz}} = 0.06$  a.u. (305 MV/cm), whereas the optical driver has linear polarization, codirected with the THz field, with 10-fs duration and field amplitude  $E_{\text{opt}} = 0.018$  a.u. (92 MV/cm), centered at 800-nm wavelength. In Fig. 1(b) the corresponding spectrum is shown for this pump configuration by the blue solid line. As one can see by a comparison to the case of the same  $E_{\text{opt}}$  but zero  $E_{\text{THz}}$  [green dashed line in Fig. 1(b)], the presence of a strong THz pump leads to a significant amplification of harmonic intensity.

Following from the previous description, the basic mechanism of these harmonics is the Brunei nonlinearity, but enhanced by the optical modulations of the ionization rate. The inset in Fig. 1(b) also shows that this intensity grows quickly with increasing  $E_{\text{opt}}$ . We see also that the Brunei harmonics decay exponentially with the harmonics number, as is known for other pump configurations [25]. Nevertheless, harmonics up to order  $\sim 7$  are still visible. In contrast to a single-pump configuration, both even and odd harmonics are present. This is the obvious consequence of the fact that the THz wave breaks the inversion symmetry of the whole system. Also, for the sake of comparison, in Fig. 1(b) (black dashed line) we plot Brunei harmonics given by the purely optical field  $E_{\text{opt}} = 0.078$  a.u. (397 MV/cm), corresponding to  $E_{\text{THz}} + E_{\text{opt}}$  in the previous configuration. Although for odd harmonics the latter case produces radiation with higher efficiency, this radiation is dominated by the bound-bound transitions. In addition, a higher number of harmonics provides an additional advantage: The possibility to produce very broad continuous spectra, as described below.

For comparison, the impact from perturbative (bound-bound) transitions in this situation is shown in Fig. 1(b) by the orange dotted line. The action of

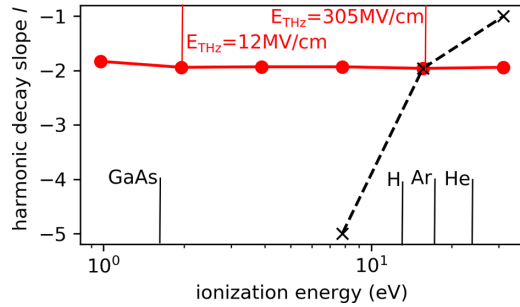


FIG. 2. Slope  $l$  in the expression  $I_r(n) \sim 10^{nl}$  as a function of the ionization energy with simultaneously rescaled frequencies, pump intensities, and durations as described in the text (red solid curve) and for fixed frequencies, pump durations, and intensities (black dashed line). Nearly constant slope indicates equivalent combs, that is, the same number of effectively radiated harmonics. Vertical lines exemplify ionization energies and band gaps of several materials (black labels) and the THz field strengths used for the simulations (red labels).

bound-bound transitions was calculated as  $dJ_{b-b}/dt = d^2P_{b-b}/dt^2 = \epsilon_0 \frac{d^2}{dt^2} \sum_j \chi^{(j)}(E_{\text{opt}} + E_{\text{THz}})^j$ , where  $\chi^{(j)} = (1 - \rho/\rho_0)\chi_0^{(j)} + \rho/\rho_0\chi_+^{(j)}$ ,  $\chi_0^{(j)}$ , and  $\chi_+^{(j)}$  are the nonlinear susceptibilities for nonionized and ionized atoms, respectively. We have taken  $j=3$  and  $5$  into account with the values [26] for argon,  $\chi_0^{(3)} = 3.5 \times 10^{-26} \text{m}^2/\text{V}^2$  and  $\chi_0^{(5)} = -2.0 \times 10^{-47} \text{m}^4/\text{V}^4$ , whereas  $\chi_+^{(j)}$  were neglected. As we see, for most harmonics and most intensities, the impact of this mechanism is one to several orders of magnitude smaller than that of the mechanism presented here. This is different from the case of only a single color, where bound-bound transitions typically overcome the action of the Brunel mechanism [26] (not shown).

Returning to the decay of harmonic intensity  $I_r(n)$  in Fig. 1(b) with the harmonic number  $n$ , we can estimate the slope  $l$  in the dependence  $I_r(n) \propto 10^{nl}$  as  $l \approx -1.93$ . On the other hand, in Fig. 1(b) we used argon with ionization energy  $V_i = 15.6 \text{ eV}$  as the model atom for which efficient excitation requires a high THz field in the 100-(MV/cm) range, which is difficult to achieve in experiments currently. We can try to reproduce this comb structure with the same number of effectively excited harmonics since lower  $V_i$  needs lower THz field intensity. To do this we repeated our simulations from Fig. 1 with varying  $V_i$ , modifying at the same time other parameters as described below. Namely, modification of  $V_i$  can be understood as rescaling  $V_i \rightarrow V_i/X$  with varying  $X$ . In these terms, together with the rescaling of  $V_i$ , we rescaled all driver frequencies as  $\omega_{\text{opt}} \rightarrow \omega_{\text{opt}}/X$ ,  $\omega_{\text{THz}} \rightarrow \omega_{\text{THz}}/X$  to keep the number of photons needed to ionize the medium fixed. In addition, we also rescaled the pulse durations  $\tau \rightarrow \tau/X$  so that every pulse contains a fixed number of cycles. Finally, we rescaled the fields as  $E_{\text{opt}} \rightarrow X^{2/3}E_{\text{opt}}$ ,  $E_{\text{THz}} \rightarrow X^{2/3}E_{\text{THz}}$  in order to keep the effective Keldysh parameters  $\gamma_j = \sqrt{2mV_i\omega_j/e|E_j|}$  for both optical and THz frequencies  $j = \{\text{opt}, \text{THz}\}$  fixed.

The result is shown in Fig. 2 (red solid line). Although, formally speaking, it is impossible to describe the ionization with

two separate Keldysh parameters, we see that the rescaling above leads, indeed, to essentially the same frequency combs, characterized by nearly the same slopes  $l$ , leading therefore to effectively the same number of harmonics in the comb. As one can see, with decreasing  $V_i$  one needs a significantly smaller THz field to generate such a comb. For instance, for  $V_i$  corresponding roughly to the band gap of GaAs, only  $\sim 10 \text{ MV/cm}$  are needed, which is much easier achievable experimentally [16].

Dramatically different from the rescaling described above, if we modify only  $V_i$ , keeping all other parameters (field amplitudes, frequencies, pulse durations) the same, decreasing  $V_i$  leads to a decrease in the number of harmonics (Fig. 2, black dashed line), visible as a significant increase of  $|l|$ .

### III. BEYOND THE DIPOLE APPROXIMATION

It is known that for the strong low-frequency pump in far-infrared and THz ranges the maximal electron velocity increases, and the terms which one might call relativistic start to play a role [27–30]. In particular, the impact of the Lorentz force due to the magnetic field of the pump grows with the pump wavelength.

The particular approximation when the magnetic field is neglected (and the corresponding Hamiltonian can be, furthermore, considered space independent) is often referred to as the dipole approximation. In the case of linearly polarized monochromatic field (with frequency  $\omega$ ) polarized in the  $x$  direction, in the dipole approximation the electron moves, therefore, along the  $x$  direction as well. On the other hand, if the magnetic field of the driving field is taken into account, the electron trajectory forms a figure eight, located in the  $x$ - $z$  plane (assuming  $z$  is the propagation direction). The maximal excursions in the  $z$  and  $x$  directions are given by  $c\zeta/8\omega$  and  $c\sqrt{\zeta}/\omega$ , respectively ( $c$  is the speed of light in vacuum); therefore, their ratio  $r_d$  is given by  $r_d = \sqrt{\zeta}/8$ , where  $\zeta = 2z_f/(1+z_f)$  and  $z_f = 2U_p/mc^2$  is related to the relativistic mass shift of the electron in the field [28],  $U_p = e^2E^2/4m\omega^2$  is the ponderomotive energy. In the other words, the parameter  $r_d$  determines the “squeezing” of the figure eight in the  $z$  direction. For instance, for the parameters in Fig. 1  $z_f \approx 0.5$ ,  $\zeta \approx 0.6$ , and  $r_d \approx 0.1$ . Although this perturbation of the electron trajectory does not seem to be too significant yet, this has a dramatic impact on the recollision harmonics since the absolute value of the excursion in the  $z$  direction is around  $2 \times 10^4 \text{ a.u.}$ , that is, much larger than the size of the atom. This leads to a significant decrease in the probability of the recollision and therefore in the amplitude of the recollision-based harmonics.

As the discussion above shows, the central mechanism in our case is however the Brunel nonlinearity. In contrast to the recollision-based harmonics, Brunel harmonics are known not to decrease but, in contrast, to increase with the driving wavelength [31,32] due to several effects, in particular, because of the increasing of the electron acceleration.

To inspect more closely the influence of the nondipole effects described in the previous paragraphs we consider the trajectory of a classical electron, born due to ionization at some exemplary time  $t_0$  at the point  $\mathbf{r} = 0$  and driven with

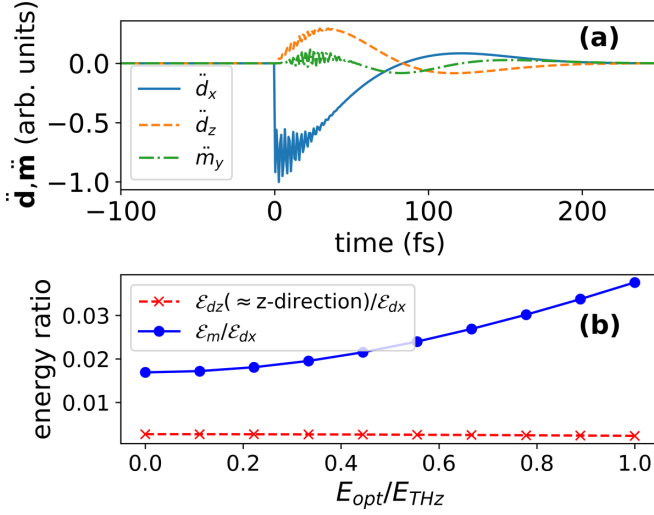


FIG. 3. Radiation in the dipole approximation and beyond from a classical electron born at  $t = 0$  with zero initial velocity. (a) Nonzero components of the second derivatives of the electric  $\mathbf{d}$  and magnetic  $\mathbf{m}$  dipoles as a function of time for the parameters in Fig. 1. The other components related to the dipole and quadrupole electric and dipole magnetic moments are negligible. (b) Ratios of energy radiated by the electric dipole component  $d_z$  in the  $z$  direction  $\mathcal{E}_{dz}$  (red dashed line) and of the energy radiated by the dipole magnetic momentum  $\mathcal{E}_m$  (blue solid line) to the energy  $\mathcal{E}_{dx}$  radiated by the electric dipole component  $d_x$ .

the field according to

$$\ddot{\mathbf{r}} = eE + e\mathbf{v} \times \mathbf{B}, \quad (2)$$

where the dots mean the time derivative,  $\times$  denotes the cross product,  $\mathbf{r} = \mathbf{r}(t)$  describes the time-dependent electron position,  $\mathbf{v} = \dot{\mathbf{r}}$  is the electron velocity, and  $\mathbf{B}$  is the magnetic field of the driving pulse. In the same approximation as Eq. (1), that is, neglecting the size of the system (which also assumes neglecting the electron excursion compared to the radiation wavelength), radiation, produced by the electron and measured at the position  $\mathbf{R}_0$ , is given by

$$\mathbf{E}_r = \frac{4\pi\epsilon_0}{c^2 R_0} (\ddot{\mathbf{d}} \times \mathbf{n}) \times \mathbf{n}, \quad (3)$$

where  $R_0 = |\mathbf{R}_0|$ ,  $\mathbf{n} = \mathbf{R}_0/|\mathbf{R}_0|$  and  $\mathbf{d} = e\mathbf{r}$  is the dipole moment of the resulting electron-ion pair (we assume that the ion remains at  $\mathbf{r} = 0$ ).

Note that neglecting the size of the radiating system compared to the radiation wavelength is also called the dipole approximation [27]. In contrast to the dipole approximation mentioned earlier in this section, this approximation is related to the overall size of the radiating system rather than the details of the electron movement and describes the properties of the radiated field rather than the properties of the electron motion.

For the same driving field as in Fig. 1, Fig. 3(a) gives nonzero components of  $\ddot{\mathbf{d}}$  produced during the electron motion according to Eq. (2), assuming the electron is born at the most probable position—the center of the pulse  $t_0 = 0$  [see Fig. 1(a)]. One can see that the component of the dipole moment corresponding to the movement along the  $z$  direction,

which arises because of the influence of the magnetic field of the pump, is already compatible with the  $x$  component, which appears due to the action of the driving electric field. However, because of the angular radiation diagram of this particular dipole component  $I(\theta) \propto \sin^2 \theta$ , where  $\theta$  is the angle to the  $z$  axis, if we measure radiation close to the  $z$  axis, the  $z$  component is less visible. More quantitatively, the ratio of energies  $r_{\mathcal{E}_d}$  radiated into a cone defined by a small angle  $\delta$  to the  $z$  axis by these two dipoles therefore can be estimated as  $r_{\mathcal{E}_d} = \frac{\delta^2}{2} \frac{\mathcal{E}_{dz}}{\mathcal{E}_{dx}}$ , where  $\mathcal{E}_{dj} = \int (\ddot{d}_j)^2 dt$ ,  $j = \{x, z\}$ ,  $d_j$  is  $j$ th component of  $\mathbf{d}$ . This ratio is shown in Fig. 3(b) by the red dashed line for  $\delta = 10^\circ$ . One can see that, despite the relatively large angle  $\delta$ , this ratio is still below  $10^{-2}$  for the parameters we consider.

Furthermore, the electron excursion in the  $x$  direction for the parameters in Fig. 1 is already around  $10 \mu\text{m}$ , which is much larger than the wavelength of the optical field and only 10 times smaller than the wavelength of the THz field we consider here. Further terms in the decomposition to the powers of  $a/\lambda$ , where  $a$  is the system size (in our case it must include the full excursion) and  $\lambda$  is the radiated wavelength, must be taken into account [27]. That is, we must go beyond the dipole radiation decomposition in Eq. (3). The corresponding extended equation including the next two terms, the so-called magnetic dipole and the electric quadrupole, is given by [27]

$$\mathbf{E}_r = \frac{4\pi\epsilon_0}{c^2 R_0} \left\{ (\ddot{\mathbf{d}} \times \mathbf{n}) \times \mathbf{n} + \frac{1}{6c} (\ddot{\mathbf{D}} \times \mathbf{n}) \times \mathbf{n} + \ddot{\mathbf{m}} \times \mathbf{n} \right\}, \quad (4)$$

where  $\mathbf{m} = \frac{1}{2c} \mathbf{r} \times \mathbf{v}$  is the magnetic dipole momentum and vector  $\mathbf{D}$  is defined as  $D_j = D_{ij} n_j$  via components  $n_j$ ,  $j = \{x, y, z\}$ , of  $\mathbf{n}$  and via the electric quadrupole tensor  $D_{ij} = e(3r_i r_j - \delta_{ij} r^2)$ , where  $r_i$  and  $r_j$  are the components of  $\mathbf{r}$ ,  $\delta_{ij}$  is the Kronecker delta and  $r^2 = |\mathbf{r}|^2$ .

For the parameters in Fig. 1 our simulations show that the amplitude of radiation caused by the electric quadrupole is around 14 orders of magnitude smaller than that from the electric dipole and therefore is completely negligible. The only nonzero component is  $m_y$ , shown by the green dot-dashed line in Fig. 3(a). One can see that its amplitude is already only one order of magnitude smaller than the dipole contributions. The term  $\ddot{\mathbf{m}}$ , representing nonzero magnetic dipole, is shown in Fig. 3(a). This component does radiate a significant amount of energy in the  $z$  direction, which we, as already mentioned, consider the observation direction. Nevertheless, the ratio of energies emitted by the electric dipole (more specifically, its  $x$  component) and by the magnetic dipole is still below 0.1, as shown in Fig. 3(b). Multipoles with yet higher orders as considered here have significantly smaller impact than the multipoles we already considered and therefore can be neglected.

Concluding this section, we see that there are non-negligible contributions beyond the dipole approximation with respect to the electron motion as well as to the radiation created by this motion. In the former case, if we observe radiation in the propagation direction, all these nondipole terms can still be neglected. This is in drastic contrast to the recollision-based harmonics, which are significantly influenced by the nondipole terms at already much lower THz fields. Therefore,

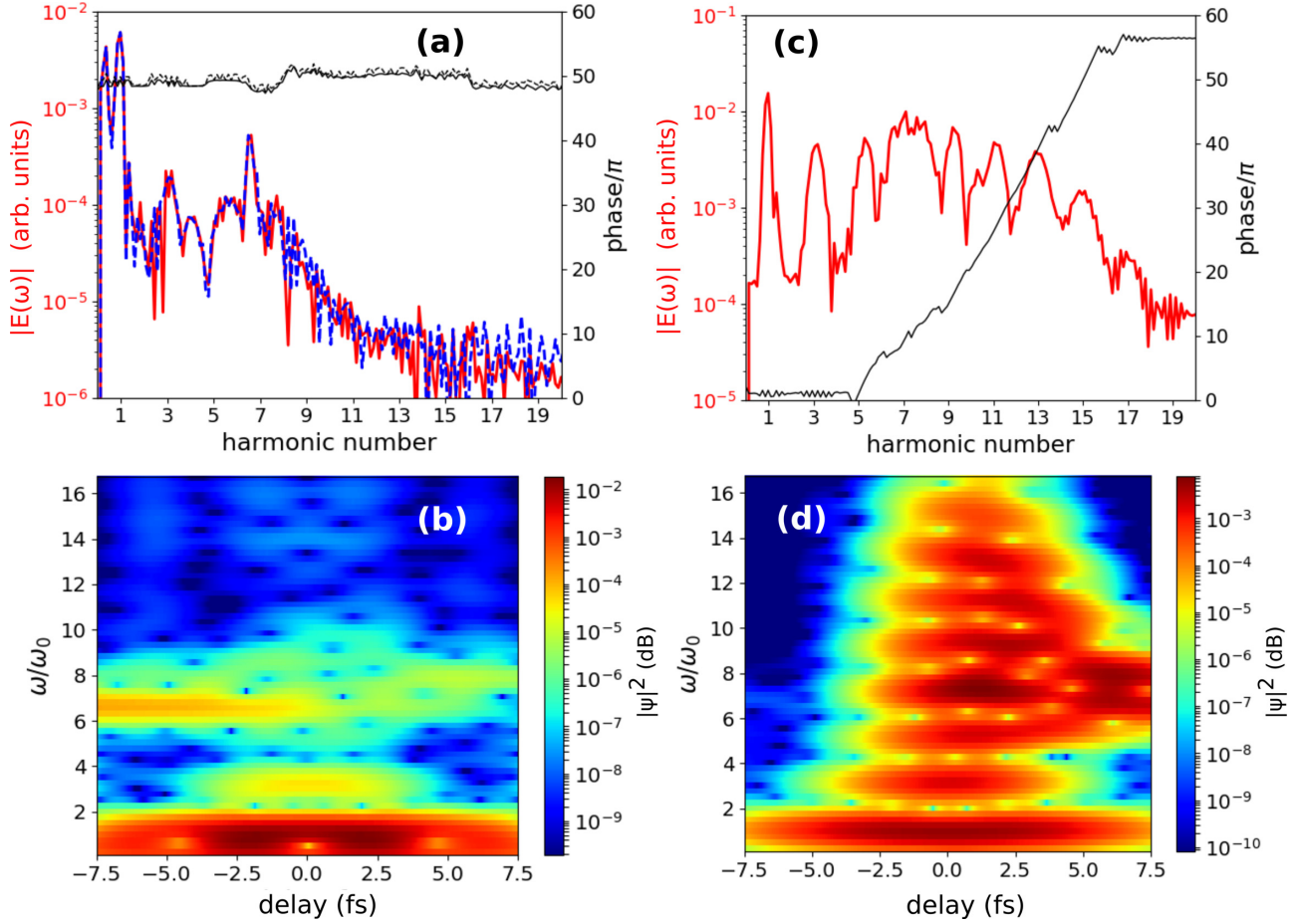


FIG. 4. The response of the hydrogen atom according to TDSE simulations [Eqs. (5) and (6)] with  $E_{\text{opt}}$  given by a 5-fs-long pulse (a) and (b) with and (c) and (d) without a strong THz field. (a) and (c) The harmonic spectrum of the atomic response  $\mathbf{E}_r$  according to Eq. (7). Spectral amplitudes for CEO phases of 0 (red solid lines) and  $\pi$  (blue dashed line) and spectral phases (black solid and dashed lines for CEO phases of 0 and  $\pi$ , respectively). (b) and (d) Corresponding XFROG traces (see text for details). Additional parameters are given in the text.

in the next sections we neglect the nondipole terms both in the electron motion and in the radiation.

#### IV. HARMONICS IN HYDROGEN USING *AB INITIO* QUANTUM SIMULATIONS

As a next step, we simulate the ionization process using the time-dependent Schrödinger equation (TDSE) for the hydrogen atom:

$$i\hbar\partial_t\psi(\mathbf{r}, t) = H\psi(\mathbf{r}, t), \quad (5)$$

$$H = \frac{1}{2m}[\mathbf{p} + e\mathbf{A}(t)]^2 + V(r), \quad (6)$$

where  $\hbar$  is the reduced Planck constant,  $\psi(\mathbf{r}, t)$  is the wave function of the electron depending on space  $\mathbf{r}$  (with  $r \equiv |\mathbf{r}|$ ) and time  $t$  coordinates,  $H$  is the electron's Hamiltonian,  $\mathbf{p}$  is the momentum operator,  $\mathbf{A}(t)$  is the vector potential of the driving field corresponding to the electric field strength  $\mathbf{E}(t) = -\partial_t\mathbf{A}$ , and  $V = -1/r$  is the potential created by the hydrogen core. The optical response of the atom, which in this case includes not only the Brunel mechanism but also bound-bound transitions and recollision harmonics, is given

by

$$\mathbf{E}_r(t) \propto \frac{d^2\mathbf{d}(t)}{dt^2}, \quad \mathbf{d}(t) = e\langle\psi|\mathbf{r}|\psi\rangle. \quad (7)$$

The code developed in [33] based on an effective scheme using expansion over spherical harmonics with space-varying coefficients was used to perform the numerical integration using a simulation box size of 500 a.u. and step size in time of 0.02 a.u. Angular harmonic numbers  $L$  and  $m$  up to 30 were used. The transmission-free absorbing potential [34] was used to treat the boundaries. The correction of the dipole  $\mathbf{d}$  due to absorption in the potential  $d^2\mathbf{d}/dt^2 \rightarrow d^2\mathbf{d}/dt^2 + \mathbf{E}(t)[1 - \|\psi(\mathbf{r}, t)\|]$ , where  $\|\psi(\mathbf{r}, t)\|$  is the norm of the electron wave function, was taken into account to avoid spurious Brunel harmonics arising due to absorption..

In the description equations (5), (6), and (7), nondipole terms in both electron motion and radiation are neglected; however, this is still a reasonable approximation, as shown in the previous section. The simulations were checked for convergence by considering different box and step sizes and

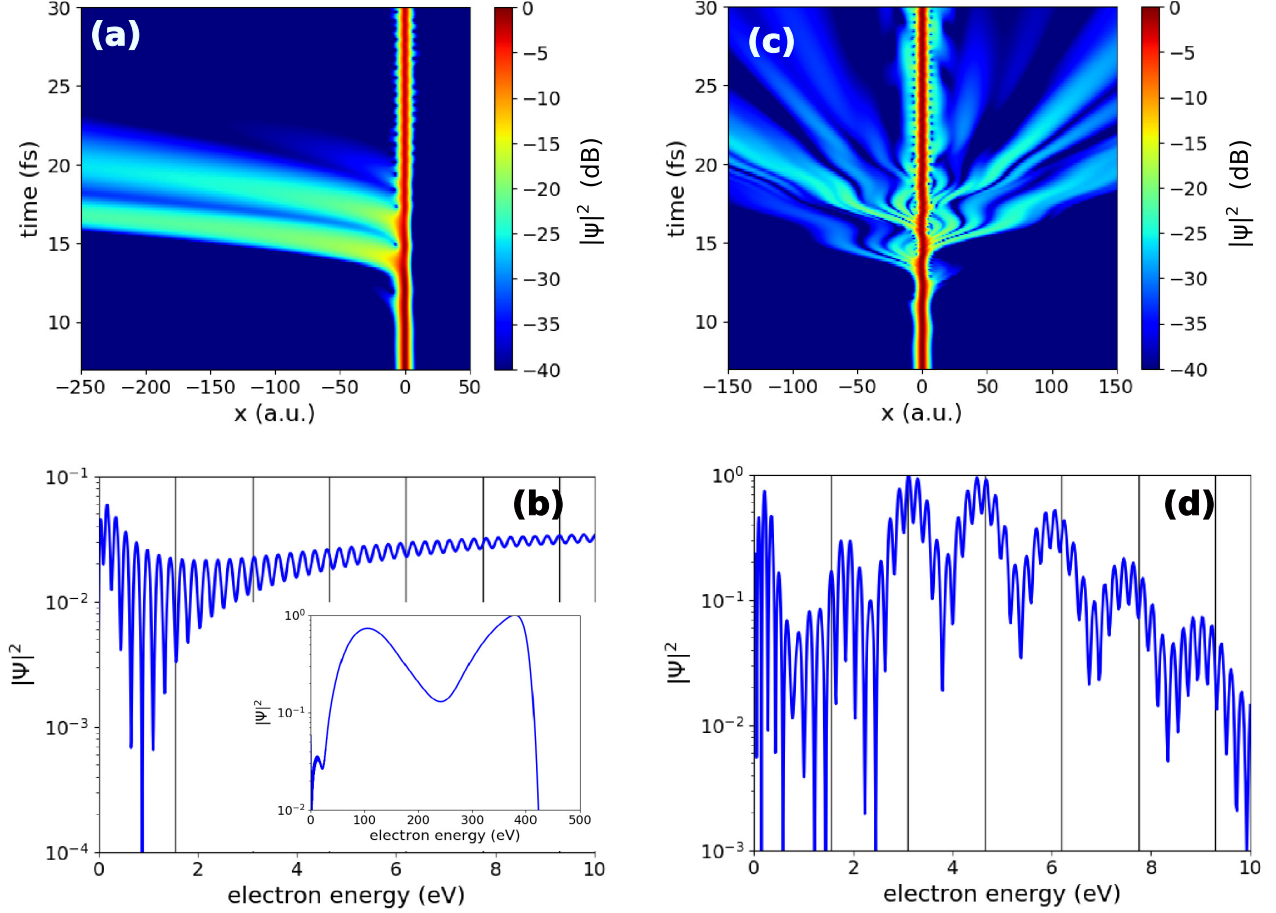


FIG. 5. (a) and (c) Spatiotemporal dynamics of the electron wave packet  $|\psi(x,t)|^2$  simulated by 1D TDSE with the soft-core potential (a) for the THz+optical field and (c) for only the optical pump. (b) and (d) The corresponding PESs calculated after the end of the pulse. The inset in (b) shows the corresponding PESs on a larger energy scale. The parameters are the same as in Fig. 4.

numbers of harmonics. The driving field was given by  $\mathbf{A} = \mathbf{A}_{\text{THz}} + \mathbf{A}_{\text{opt}}$ ,

$$A_{x,\text{opt}} = A_{0,\text{opt}} e^{-\frac{t^2}{\tau^2}} \sin(\omega_{\text{opt}} t), \quad (8)$$

$$A_{x,\text{THz}} = A_{0,\text{THz}} e^{-\frac{t^2}{\tau^2}} \sin(\omega_{\text{THz}} t), \quad (9)$$

$$A_{y,\text{opt}} = 0, \quad A_{y,\text{THz}} = 0, \quad (10)$$

where  $\omega_{\text{opt}}$  is the frequency corresponding to 800-nm wavelength and  $\omega_{\text{THz}} = 3 \times 2\pi$  rad/ps and  $\tau$  corresponds to 5-fs FWHM.

The results of the simulation for the hydrogen atom,  $E_{\text{THz}} = 0.03$  a.u. and  $E_{\text{opt}} = 0.012$  a.u., are shown in Figs. 4(a) and 4(b). Figure 4(a) shows the spectrum of  $\mathbf{E}_r$  for two different carrier-envelope (CEO) phases, 0 and  $\pi$ , and in Fig. 4(b) the cross-correlated optical frequency-resolved gating (XFROG) trace for the zero CEO phase is presented, defined as  $I_{\text{XFROG}}(\omega, \tau) = |\int E(t) E_{\text{ref}}(t - \tau) e^{-i\omega\tau}|$  with integration from  $-\infty$  to  $+\infty$ , with  $E(t)$  being the tested field and  $E_{\text{ref}}(t - \tau)$  being the reference pulse taken in the form of a Gaussian shape with 2.7-fs FWHM duration. For comparison, in Figs. 4(c) and 4(d) the same pictures are shown for only the strong optical pump ( $E_{\text{opt}} = 0.033$  au). As one can see,

in the latter case high-order harmonics up to  $\sim 17$  appear. Examining the XFROG [Fig. 4(d)], we see that these harmonics originate from the recollision mechanism. This is indicated by the characteristic time-dependent delay [35] in harmonic emission visible in Fig. 4(d). In contrast, in the case of THz+optical pump the harmonics have no systematic delay; that is, they are created instantaneously, pointing clearly to the non-recollision-based mechanism. We see also that the harmonics are less localized in time in the two-color case, which is also well explained by the Brunel mechanism since the Brunel harmonics are born in the process of both electron birth and acceleration, so their generation takes a certain amount of time. The different generation mechanism is furthermore indicated by radically different spectral phases for two- and single-color cases, shown by the black lines in Figs. 4(a) and 4(d). The former is almost frequency independent, in strong contrast to the latter. The spectrum in the two-color case is extended only up to around the 10th harmonic, in qualitative agreement with the simple-man theory [see Fig. 1(b)], therefore also supporting the Brunel nonlinearity as the leading mechanism.

This suggests that the recollision-based harmonics are significantly suppressed even in the dipole approximation. To obtain additional confirmation of this, we made simulations

of one-dimensional variant of Eqs. (5) and (6) with a soft-core Coulomb potential  $V = -1/\sqrt{x^2 + a^2}$ , which for  $a = 1/\sqrt{2}$  has the same ionization potential as the hydrogen atom [36,37] and  $x$  is the spatial coordinate. The results of simulations for the same parameters as in Figs. 4(a) and 4(d) are given in Figs. 5(a) and 5(b), respectively. The advantage of the one-dimensional simulation is that one can very clearly see the trajectories of the electrons: If the strong THz field is present [Fig. 5(a)], the electrons move from the core without undergoing even a single recollision, in strong contrast to the case of the single-color optical pump [Fig. 5(b)]. This is explained by the fact that the ponderomotive energy gained by the electron from the THz field over the half of the optical field cycle  $\propto E_{\text{THz}}^2 \lambda_{\text{opt}}^2$ , which is one order of magnitude larger than the energy gained from the optical field  $\propto E_{\text{opt}}^2 \lambda_{\text{opt}}^2$  over the same time (half cycle of the optical pulse  $\lambda_{\text{opt}}/2$ ). Because the subsequent optical half cycles are located within the very same THz cycle, the electron has no chance to return.

We find it instructive to look at the photoelectron spectra (PESs) after the pulse, which are shown in Figs. 5(b) and 5(d). PESs were obtained by extracting the part of the wave function  $\psi_i(\mathbf{r})$  orthogonal to the wave function of the fundamental bound state and transforming it into the momentum space  $\psi_i(\mathbf{p})$ , which gives the corresponding energy distribution  $|\psi_i(\mathbf{p}(h))|^2$ ,  $h = |\mathbf{p}|^2/2m$ .

We see [Fig. 5(d)] that for the single-color optical pump, the PES has a width of the order of 10 eV. Fast, sub-eV-scale oscillations are most likely the effect of the slow pulse envelope. The spectrum is also modulated on the eV scale, with several peaks close to the multiples of the optical pump energy  $n\hbar\omega_{\text{opt}}$ . We note that these multiphoton channels appear on the multicycle timescale as a result of interference between different electronic wave packets [38,39]. The effect of such intercycle interference is also visible in real space [Fig. 5(d)]. We note that it is not possible to distinguish which multiphoton channel is active if we look at only the subcycle scale since for small time intervals the energy of the electron is not defined.

However, in the optical case it is still possible to make a decision about the leading ionization channel by looking at the PESs after the end of the driving pulse. In our case, the ionization energy  $V_i = 13.6\text{eV}$  would correspond, in the multiphoton regime, to nine-photon ionization; therefore, the presence of only the lowest multiphoton channels  $n \ll 9$  shows that we are not in the multiphoton regime anymore; tunneling would be a much better description.

In contrast, in the presence of strong THz field [Fig. 5(b)] there is no interference between the parts of wave packets ionized at different positions in time anymore since they are quickly separated also in space. Therefore, there are also no multiphoton peaks appearing in PESs after the pulse. The spectrum is therefore flat (except for the sub-eV oscillations mentioned above) and extends up to the ponderomotive energy  $U_p$  [see inset in Fig. 5(b)], which is, in this case, significantly higher than for the single-color optical driver. This flat PES indicates that the tunneling (rather than multiphoton) ionization picture is a suitable description in this situation [see inset in Fig. 1(a)].

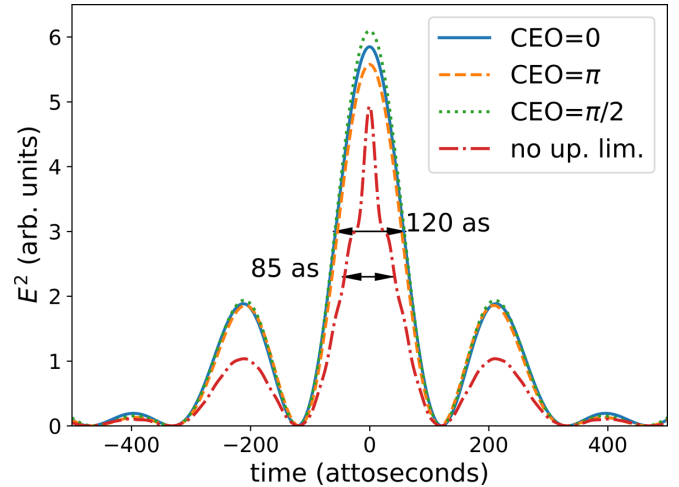


FIG. 6. The square of the electric field depending on time for the Fourier-limited pulse obtained from the spectrum in Fig. 4(a) in the range between  $\omega = 1.5\omega_0$  and  $\omega = 10\omega_0$  (solid blue line). The FWHM duration of the resulting pulse is 120 as. To demonstrate the CEO insensitivity, the dashed orange and dotted green lines show the cases of the different CEO phases of the optical driver, compressed with the phase mask for the zero CEO phase. The red dash-dotted line shows the compressed pulse with the same lower but no upper frequency filtering limit. In this case the FWHM duration is 85 fs.

## V. SUPERCONTINUUM AND ISOLATED ATTOSECOND PULSES IN HYDROGEN

Importantly, the spectrum in Fig. 4(a) forms a broad continuum in the range of  $n \approx 1.5-9$  harmonics. The most important reason why separate harmonics join into a broad continuum is the short optical probe, leading to broadening of every harmonic. Further, in our case both odd and even harmonics are present, so the distance between the subsequent harmonics is 2 times smaller than in a single-color case. The spectral phase of the resulting continuum is very flat across the whole spectral range [see black lines in Fig. 4(a)]. Removing this phase leads to a stand-alone Fourier-limited compressed pulse of 100-as duration, as shown in Fig. 6. If the spectral range from the 1.5th to 10th harmonic is taken for compression, the resulting pulse is 120 as long, whereas if the whole spectrum above 1.5th harmonic is used, the final pulse duration is reduced to 85 as.

Quite remarkably, both the spectral intensity and the spectral phase are rather insensitive to the CEO phase of the optical probe [see Fig. 4(a), where the cases for different CEO phases are shown by solid and dashed lines]. This is in strong contrast to the continua created by recollision-based harmonics (which are also located at higher frequencies) [40–42]. These continua are heavily CEO dependent since they rely on the intercycle electron trajectories leading back to the core. In contrast, the Brunel radiation is emitted during the ionization event, taking place on subcycle scales. Interestingly, the CEO insensitivity of the continuum is also rather different from the behavior of separate harmonics obtained from longer pump pulses [for instance, in Fig. 1(b)] where the CEO phase of the  $n$ th harmonic is  $n$  times the CEO phase of the fundamental.

This pronounced CEO insensitivity leads also to the insensitivity of the resulting compressed pulse to the CEO phase, as shown in Fig. 6, where compression of the spectra resulting from an optical probe with different CEO phases is performed using the same phase mask. That is, the compression scheme does not require CEO stabilization of the optical probe. As we can see, these pulses also do not require the gating necessary for isolating attosecond pulses for recollision-based harmonics [40–42].

## VI. CONCLUSION AND DISCUSSION

In conclusion, we showed that in the presence of an extreme almost ionizing THz driver, higher-order harmonics can be generated by a weak optical probe pulse via the Brunel (ionization-induced) mechanism. This mechanism dominates over the recollision-based one since the recollisions are strongly suppressed in the presence of the strong THz field. The efficiency of the generated harmonics is, in our case, comparable to the recollision-based ones. To avoid the phase-matching and nonlinear-pump-propagation issues (neglected in our consideration), dilute gases can be considered, which might reduce the efficiency.

When considering the generation of such harmonics in hydrogen driven by a few-cycle optical pump, the harmonics in the range from visible to XUV are “glued” together, forming a broadband supercontinuum, compressible to an isolated 100-as-scale pulse without the need for gating techniques. Importantly, the resulting supercontinuum is fully insensitive to the CEO phase of the optical driver, so CEO stabilization is not required. CEO-phase insensitivity also implies shot-to-shot coherence of the supercontinuum, the property which is

difficult to achieve using traditional fiber-based supercontinuum generation methods [43–45].

Although we focused in this paper on considering atomic media, in particular the hydrogen atom, the resulting harmonic combs are scalable to lower ionization energies if the driving field intensities and frequencies are decreased accordingly. Our results preliminarily indicate that similar harmonic combs and therefore supercontinua are possible in semiconductors with eV-scale band gaps. In that case, the THz field strengths required for excitation of the combs can be around tens of megavolts per centimeter.

The Brunel harmonic spectrum reflects energy band structure [46] and should be sensitive to the mutual orientation of both the field polarization and crystal lattice. Thus, the generated Brunel harmonics might be used as a sensitive tool for time-resolved studies of the energy bands in solids under the action of an extreme THz field with strength well above the dc field breakdown threshold. Here it is important that the probing optical field might be  $10^{12}$  W/cm<sup>2</sup> or lower and does not disturb the sample.

## ACKNOWLEDGMENTS

A.S. acknowledges support from the Russian Science Foundation under Project No. 20-19-00148. I.B. and U.M. thank Deutsche Forschungsgemeinschaft (DFG, German Research Foundation), under Projects No. BA 4156/4-2 and No. MO 850-19/2, for support. I.B., A.D., and U.M. acknowledge support from Germany’s Excellence Strategy within the Cluster of Excellence PhoenixD (EXC 2122, Project No. 390833453).

- [1] C. Vicario, B. Monoszlai, and C. P. Hauri, GV/m Single-Cycle Terahertz Fields from a Laser-Driven Large-Size Partitioned Organic Crystal, *Phys. Rev. Lett.* **112**, 213901 (2014).
- [2] A. Sell, A. Leitenstorfer, and R. Huber, Phase-locked generation and field-resolved detection of widely tunable terahertz pulses with amplitudes exceeding 100 MV/cm, *Opt. Lett.* **33**, 2767 (2008).
- [3] X. C. Zhang, A. Shkurinov, and Y. Zhang, Extreme terahertz science, *Nat. Photonics* **11**, 16 (2017).
- [4] O. Schubert, M. Hohenleutner, F. Langer, B. Urbaneck, C. Lange, U. Huttner, D. Golde, T. Meier, M. Kira, S. W. Koch, and R. Huber, Sub-cycle control of terahertz high-harmonic generation by dynamical Bloch oscillations, *Nat. Photonics* **8**, 119 (2014).
- [5] X. Chai, X. Ropagnol, A. Ovchinnikov, O. V. Chefonov, A. Ushakov, C. M. Garcia-Rosas, E. Isgandarov, M. Agranat, T. Ozaki, and A. Savel’ev, Observation of crossover from intra-band to interband nonlinear terahertz optics, *Opt. Lett.* **43**, 5463 (2018).
- [6] M. B. Agranat, O. V. Chefonov, A. V. Ovchinnikov, S. I. Ashitkov, V. E. Fortov, and P. S. Kondratenko, Damage in a Thin Metal Film by High-Power Terahertz Radiation, *Phys. Rev. Lett.* **120**, 085704 (2018).
- [7] P. B. Corkum, N. H. Burnett, and F. Brunel, Above-Threshold Ionization in the Long-Wavelength Limit, *Phys. Rev. Lett.* **62**, 1259 (1989).
- [8] P. B. Corkum and F. Krausz, Attosecond science, *Nat. Phys.* **3**, 381 (2007).
- [9] P. B. Corkum, N. H. Burnett, and M. Y. Ivanov, Subfemtosecond pulses, *Opt. Lett.* **19**, 1870 (1994).
- [10] M.-Q. Bao and A. F. Starace, Static-electric-field effects on high harmonic generation, *Phys. Rev. A* **53**, R3723(R) (1996).
- [11] G. Vampa, T. J. Hammond, M. Taucer, X. Ding, X. X. Ropagnol, T. Ozaki, S. Delprat, M. Chaker, N. Thiré, B. E. Schmidt, F. Légaré, D. D. Klug, A. Y. Naumov, D. M. Villeneuve, A. Staudte, and P. B. Corkum, Strong-field optoelectronics in solids, *Nat. Photonics* **12**, 465 (2018).
- [12] Y. Pan, S.-F. Zhao, and X.-X. Zhou, Generation of isolated sub-40-as pulses from gas-phase CO molecules using an intense few-cycle chirped laser and a unipolar pulse, *Phys. Rev. A* **87**, 035805 (2013).
- [13] E. Balogh, K. Kovacs, P. Dombi, J. A. Fulop, G. Farkas, J. Hebling, V. Tosa, and K. Varju, Single attosecond pulse from terahertz-assisted high-order harmonic generation, *Phys. Rev. A* **84**, 023806 (2011).
- [14] O. Chefonov, A. Ovchinnikov, S. Romashevskiy, X. Chai, T. Ozaki, A. Savel’ev, M. Agranat, and V. Fortov, Giant self-induced transparency of intense few-cycle terahertz pulses in n-doped silicon, *Opt. Lett.* **42**, 4889 (2017).
- [15] O. V. Chefonov, A. V. Ovchinnikov, M. B. Agranat, V. E. Fortov, E. S. Efimenko, A. N. Stepanov, and A. B. Savel’ev,



- Nonlinear transfer of an intense few-cycle terahertz pulse through opaque  $n$ -doped Si, *Phys. Rev. B* **98**, 165206 (2018).
- [16] A. Savel'ev, O. Chefonov, A. Ovchinnikov, A. Rubtsov, A. Shkurinov, Y. Zhu, M. Agranat, and V. Fortov, Transient optical non-linearity in  $p$ -Si induced by a few cycle extreme THz field, *Opt. Express* **29**, 5730 (2021).
- [17] F. Brunel, Harmonic generation due to plasma effects in a gas undergoing multiphoton ionization in the high-intensity limit, *J. Opt. Soc. Am. B* **7**, 521 (1990).
- [18] K. Zhang, K. Zhang, Y. Zhang, Y. Zhang, Y. Zhang, X. Wang, T.-M. Yan, T.-M. Yan, Y. H. Jiang, Y. H. Jiang, Y. H. Jiang, and Y. H. Jiang, Continuum electron giving birth to terahertz emission, *Photonics Res.* **8**, 760 (2020).
- [19] Z. Zhou, D. Zhang, Z. Zhao, and J. Yuan, Terahertz emission of atoms driven by ultrashort laser pulses, *Phys. Rev. A* **79**, 063413 (2009).
- [20] T. Balčiūnas, D. Lorenc, M. Ivanov, O. Smirnova, A. Zheltikov, D. Dietze, K. Unterrainer, T. Rathje, G. Paulus, A. Baltuška *et al.*, CEP-stable tunable THz-emission originating from laser-waveform-controlled sub-cycle plasma-electron bursts, *Opt. Express* **23**, 15278 (2015).
- [21] I. Babushkin, C. Brée, C. M. Dietrich, A. Demircan, U. Morgner, and A. Husakou, Terahertz and higher-order Brunel harmonics: From tunnel to multiphoton ionization regime in tailored fields, *J. Mod. Opt.* **64**, 1078 (2017).
- [22] L. Keldysh *et al.*, Ionization in the field of a strong electromagnetic wave, *Sov. Phys. JETP* **20**, 1307 (1965).
- [23] K.-Y. Kim, Generation of coherent terahertz radiation in ultrafast laser-gas interactions, *Phys. Plasmas* **16**, 056706 (2009).
- [24] I. Babushkin, S. Skupin, and J. Herrmann, Generation of terahertz radiation from ionizing two-color laser pulses in Ar filled metallic hollow waveguides, *Opt. Express* **18**, 9658 (2010).
- [25] I. Babushkin, S. Skupin, A. Husakou, C. Köhler, E. Cabrera-Granado, L. Bergé, and J. Herrmann, Tailoring terahertz radiation by controlling tunnel photoionization events in gases, *New J. Phys.* **13**, 123029 (2011).
- [26] U. Sapaev, A. Husakou, and J. Herrmann, Combined action of the bound-electron nonlinearity and the tunnel-ionization current in low-order harmonic generation in noble gases, *Opt. Express* **21**, 25582 (2013).
- [27] L. D. Landau and E. M. Lifshitz, *The Classical Theory of Fields* (Pergamon, New York, 2013).
- [28] H. Reiss, Theoretical methods in quantum optics: S-matrix and Keldysh techniques for strong-field processes, *Prog. Quantum Electron.* **16**, 1 (1992).
- [29] B. Wolter, M. G. Pullen, M. Baudisch, M. Sclafani, M. Hemmer, A. Senftleben, C. D. Schröter, J. Ullrich, R. Moshhammer, and J. Biegert, Strong-Field Physics with Mid-IR Fields, *Phys. Rev. X* **5**, 021034 (2015).
- [30] E. Pisanty, D. D. Hickstein, B. R. Galloway, C. G. Durfee, H. C. Kapteyn, M. M. Murnane, and M. Ivanov, High harmonic interferometry of the Lorentz force in strong mid-infrared laser fields, *New J. Phys.* **20**, 053036 (2018).
- [31] A. Nguyen, P. G. de Alaiza Martínez, J. Déchard, I. Thiele, I. Babushkin, S. Skupin, and L. Bergé, Spectral dynamics of THz pulses generated by two-color laser filaments in air: The role of Kerr nonlinearities and pump wavelength, *Opt. Express* **25**, 4720 (2017).
- [32] M. Clerici, M. Peccianti, B. E. Schmidt, L. Caspani, M. Shalaby, M. Giguère, A. Lotti, A. Couairon, F. Légaré, T. Ozaki, D. Faccio, and R. Morandotti, Wavelength Scaling of Terahertz Generation by Gas Ionization, *Phys. Rev. Lett.* **110**, 253901 (2013).
- [33] S. Patchkovskii and H. Muller, Simple, accurate, and efficient implementation of 1-electron atomic time-dependent Schrödinger equation in spherical coordinates, *Comput. Phys. Commun.* **199**, 153 (2016).
- [34] D. E. Manolopoulos, Derivation and reflection properties of a transmission-free absorbing potential, *J. Chem. Phys.* **117**, 9552 (2002).
- [35] K. Varjú II, Y. Mairesse, B. Carré, M. B. Gaarde, P. Johnsson, S. Kazamias, R. López-Martens, J. Mauritsson, K. Schafer, P. Balcou *et al.*, Frequency chirp of harmonic and attosecond pulses, *J. Mod. Opt.* **52**, 379 (2005).
- [36] J. H. Eberly, Q. Su, and J. Javanainen, Nonlinear Light Scattering Accompanying Multiphoton Ionization, *Phys. Rev. Lett.* **62**, 881 (1989).
- [37] R. L. Hall, N. Saad, K. D. Sen, and H. Ciftci, Energies and wave functions for a soft-core Coulomb potential, *Phys. Rev. A* **80**, 032507 (2009).
- [38] H. Zimmermann, S. Patchkovskii, M. Ivanov, and U. Eichmann, Unified Time and Frequency Picture of Ultrafast Atomic Excitation in Strong Laser Fields, *Phys. Rev. Lett.* **118**, 013003 (2017).
- [39] L. Shi, I. Babushkin, A. Husakou, O. Melchert, B. Frank, J. Yi, G. Wetzel, A. Demircan, C. Lienau, H. Giessen *et al.*, Femtosecond field-driven on-chip unidirectional electronic currents in nonadiabatic tunneling regime, *Laser Photonics Rev.* **15**, 2000475 (2021).
- [40] I. P. Christov, M. M. Murnane, and H. C. Kapteyn, High-Harmonic Generation of Attosecond Pulses in the "Single-Cycle" Regime, *Phys. Rev. Lett.* **78**, 1251 (1997).
- [41] T. Brabec and F. Krausz, Intense few-cycle laser fields: Frontiers of nonlinear optics, *Rev. Mod. Phys.* **72**, 545 (2000).
- [42] M. Chini, K. Zhao, and Z. Chang, The generation, characterization and applications of broadband isolated attosecond pulses, *Nat. Photonics* **8**, 178 (2014).
- [43] A. Demircan and U. Bandelow, Supercontinuum generation by the modulation instability, *Opt. Commun.* **244**, 181 (2005).
- [44] J. M. Dudley, G. Genty, and S. Coen, Supercontinuum generation in photonic crystal fiber, *Rev. Mod. Phys.* **78**, 1135 (2006).
- [45] I. Babushkin, A. Tajalli, H. Sayinc, U. Morgner, G. Steinmeyer, and A. Demircan, Simple route toward efficient frequency conversion for generation of fully coherent supercontinua in the mid-IR and UV range, *Light Sci. Appl.* **6**, e16218 (2017).
- [46] A. Lanin, E. Stepanov, A. Fedotov, and A. Zheltikov, Mapping the electron band structure by intraband high-harmonic generation in solids, *Optica* **4**, 516 (2017).